JOURNAL OF COMPUTATIONAL PHYSICS **128,** 301–318 (1996)
ARTICLE NO. 0212

A Second-Order Accurate Capturing Scheme for 1D Inviscid Flows of Gas and Water with Vacuum Zones

H. S. TANG* AND D. HUANG

Department of Mathematics, Peking University, Beijing 100871, China

Received September 24, 1993; revised May 29, 1996

A second-order accurate difference scheme is developed to study cavitation in unsteady, one-dimensional, inviscid, compressible flows of water with gas. The scheme can capture shock waves, interfaces separating gas and water, as well as cavitation zones that are modelled as vacuum states, and it takes into account water's capability to resist tensile stresses. As an extended version of the standard MUSCL scheme, this scheme is based on the solutions of local gas–water–vacuum initial value problems. In order to prevent the computed water density from becoming lower than its minimum bound, additional techniques are introduced. Numerical results are presented with gas–water Riemann problems to demonstrate the performance of the scheme. The scheme is also applied to simulate the cavitation process of the flow in a water shock tube.

1. INTRODUCTION

Fluid-flows with cavitation are of practical importance. One example is the flow generated by an underwater explosion near the sea surface. Explosion in water has already been investigated in a number of previous studies. Sedov [1] derived analytical solutions to underwater explosions. Cole [2] studied the phenomenon both theoretically and experimentally. A survey of these early studies was given by Holt [3]. Numerical methods, such as the method of characteristics and shock fitting [4, 5], have also been used to understand explosions in water that were usually beyond the reach of analytical methods. More recently, the Glimm scheme was applied to calculate the initial stage of the flow due to an explosion in shallow water [6], and a first-order accurate difference scheme was proposed to predict the one-dimensional motion of a continuum with cracks [7]. A further task on simulating such flows would be the development of numerical methods with high accuracy, as well as the capacity to capture gas–water interfaces and cavitation zones.

The flow in a water shock tube, designed to calibrate sensors for transient explosion pressure, was generated by an explosion of a small amount of dynamite [8] and was simulated numerically to clarify certain peculiar features observed in experiments [9]. In the simulation, the flow was assumed to be one-dimensional, the interface separating the water and the high pressure gaseous products of the dynamite was treated as an interior boundary, and, as a starting trial, a TVNI scheme proposed by Harten [10] with moving grids was adopted. However, computations indicated that numerical resolution for shock waves in the water was diminished due to the smearing of the shock fronts, and there was a tendency for the onset of cavitation in the water. It became necessary, as a consequence, to construct a high-order numerical method with the capability of capturing interfaces and resolving regions of flow cavitation, and, in view of some experiments, the method should also be able to model the water's capacity to resist tensile stresses.

Since the late 1970's, there have been substantial achievements in the development of difference schemes with high resolution for capturing shock waves in inviscid flows governed by hyperbolic systems of conservation laws. However, standard shock capturing methods, including those high resolution schemes, have trouble dealing with gas–water interfaces. To predict a flow composed of a gas and water, Eulerian-based difference schemes would inevitably face the difficulties that arise in mixed-cells, in which both the gas and water are present. Difficulties are also encountered in Lagrangian formulation because the density jumps at the interfaces are large and the equations of state for the gas and water are totally different. When vacuum states occur, further difficulties will arise. A vacuum is a possible solution state of the Riemann problem for the ideal gas, and there have been theoretical interests about it [11, 12]. Nevertheless, a vacuum state is usually not taken into consideration in numerical computations, since it is an extreme state and can hardly be realized (see Gottlieb and Groth [13]). In fact, in the simulation of a gas flow from rarefied to vacuum state, errors in the form of numerical oscillations may turn the computed density

* Present address: Tang Han-song, School of Space Technology, Beijing University of Aeronautics and Astronautics, Beijing 100083, China.

0021-9991/96 $18.00

or pressure to negative and thus terminate the computation. As asserted in a book edited by Babenko [14], it is impossible in principle to describe a flow from rarefied to vacuum state in the Lagrangian reference frame.

In his pioneering work [15], Godunov used exact solutions of local Riemann problems to construct his famous first-order monotone scheme. Basing it on this scheme, van Leer established the standard MUSCL scheme [16], one of the first second-order difference schemes with high resolution for shock waves. The objective of the present paper is to develop a second-order accurate capturing method for inviscid flows with gas–water interfaces and cavitation zones. However, there are some difficulties to overcome. First, the standard MUSCL scheme, originally designed for the flow of a continuous gas phase, should be extended to the present case. The extended scheme, called E-MUSCL scheme, will be presented in a second-order accurate form in the Lagrangian reference frame. Second, in order to take the capability for supporting the tensile stresses into consideration that characterizes the nature of the water, a new kind of solution to the Riemann problem has to be constructed. The wave system of this solution does not fall into any category of the five possible resolved wave systems of the Riemann problem for the ideal gas. Third, some recipes named as "algorithms for lower bound of density" are needed to keep water density higher than its minimum bound in simulating flows from a rarefied to a ruptured state. In this paper, it is proven that the solution to the gas–water–vacuum Riemann problem with given initial conditions exists uniquely, and, if the solution contains no vacuum, the iterative procedure we employ, similar to the one used by Flores and Holt [6], converges to the solution. It is also shown that the time derivatives involved in construction of the E-MUSCL scheme have unique solutions. Yet, similar to the method of [6], our approach can capture gas–water interfaces. Furthermore, the latter possesses second-order accuracy in general and, as the local Riemann problems we adopt may have solutions containing vacuum states, it can handle a flow with multiple vacuum zones.

This paper is organized as follows: Governing equations and a cavitation model are presented in Section 2. In Section 3, it follows the discussions of the relevant Riemann problems and the existance and uniqueness of their solutions. These solutions are solved with an exact Riemann solver. In Section 4, formulas for the time derivatives of intermediate solution states are presented. Then in Section 5, a description of the basic algorithm for the E-MUSCL scheme is given. Section 6 contains the algorithms for lower bound of density. In Section 7, numerical solutions to gas–water Riemann problems are displayed to demonstrate the accuracy and high resolution of the method proposed in this paper. Also in this section, the unsteady flow in the water shock tube is simulated, and some discussions on its interesting phenomenon related to cavitation are then presented.

2. GOVERNING EQUATIONS AND CAVITATION MODEL

In Lagrangian coordinates the one-dimensional equations of motion for an inviscid, non-heat-conducting fluid can be written in conservation form

$$\frac{\partial U}{\partial t} + \frac{\partial F(U)}{\partial r} = 0, \tag{2.1}$$

where

$$U = (V, u, E), \quad F(U) = (-u, P, uP). \tag{2.2}$$

Here the independent variables are the time t and the mass coordinate r. $V = \rho_{\text{ref.}}/\rho$, $P = p/\rho_{\text{ref.}}$, $E = e + u^2/2$, where $\rho_{\text{ref.}}$ is a reference density. The dependent variables are the density ρ, the velocity u, the pressure p, and the internal energy e. Here, r is related to the space coordinate x by

$$r = \frac{1}{\rho_{\text{ref.}}} \int_0^x \rho(t, \eta)\, d\eta. \tag{2.3}$$

For an ideal gas we may write

$$p = (\gamma - 1)e\rho, \tag{2.4}$$

where γ is the ratio of the specific heats. For water, when pressure is less than 3×10^9 Pa, Tait equation reads (see [17])

$$\frac{p}{p_a} = k\left(\left(\frac{\rho}{\rho_a}\right)^{\alpha} - 1\right) + 1, \quad k = 3045, \alpha = 7.15, \tag{2.5}$$

where the subscript a refers to standard atmospheric conditions; (2.5) implies that pressure does not have a relation to specific entropy. In fact, when pressure becomes quite high, its effect cannot be neglected. We assume that (2.5) holds unless inside cavitation regions.

Cavitation, which is the disruption of what would otherwise be a continuous water phase by the presence of gas or vapor or both, may appear at the region where the pressure drops to a certain critical value p_v (the subscript v refers to cavitation conditions). The criterion may be affected by the velocity, purity, temperature, etc., and it measures the capability of the water to resist the tensile stresses. Water's incapability of supporting the tensile stresses is a well-judged engineering assumption. However, Experimental results in [18] show that water may sustain

stationary tensile stresses from -1.3×10^6 Pa up to -1.6×10^7 Pa, and transient tensile stresses from -8.1×10^5 Pa up to -3.7×10^6 Pa. As a result, $p_v \leqq 0$ for water. A cavitation zone is three-dimensional with internal pressure due to the presence of the gas and vapor. For simplicity, we make the hypotheses: (1) *p_v is a parameter and water cavitates as pressure diminishes to it*; (2) *the gas and vapor in a cavitation zone are ignored and this zone is regarded as a vacuum.* Accordingly, we modify (2.5) to

$$\frac{p}{p_a} = \begin{cases} k\left(\left(\frac{\rho}{\rho_a}\right)^{\alpha} - 1\right) + 1, & \rho > \rho_v, \\ 0, & \rho \leq \rho_v, \end{cases} \tag{2.6}$$

where ρ_v is the density corresponding to p_v. In view of the above hypotheses, water ruptures as soon as pressure diminishes to p_v, and a water segment lying between cavitation zones will move freely without force acting on each of its ends. When such a segment collides with another one, the cavitation zone between them collapses and vanishes. This cavitation model has also been employed by other authors [19]. However, the model is not precise. For instance, the gas and vapor in a cavitation zone may induce some dynamic responses, such as the cavitation decaying in such a way that its size decreases in an oscillatory manner. Since the cavitation model ignores the presence of gas and vapor, it cannot simulate this process. We should also notice that in reality the behaviour of either the gas or the water near a vacuum state departs significantly from those described by (2.4) or (2.6). As a consequence, governing equations for water phase consists of (2.6) and the first two equations in (2.1). Hence there are only two coupled nonlinear differential equations in water, while in the gas phase there are three. Additionally, the fact that gas cannot sustain tensile stresses will be treated as $p_v = 0$ for gas.

3. RIEMANN PROBLEM AND ITS SOLUTION

3.1. *Resolution of the Riemann Problem*

The governing equations (2.1) are a hyperbolic system of conservation laws. We will discuss the Riemann problem of (2.1), or the initial value problem for the system (2.1) with initial conditions given by the step function

$$U_{t=0} = \begin{cases} H_l, & r < 0, \\ H_r, & r > 0, \end{cases} \tag{3.1}$$

where $H = (V, u, P)$, the subscripts l and r denote the left and right side of $r = 0$, respectively, and the medium to the left and right of $r = 0$ may be water or gas, or may be a vacuum zone. A Riemann problem of a hyperbolic system comprised by n scalar conservation laws in n unknowns has a solution that consists of $n + 1$ constant states connected by n centered waves, provided that initial values on one side of initial discontinuity belong to a neighborhood of the ones on the other side [20]. The above gas–water–vacuum Riemann problem is classified into four categories and its solution will be discussed as follows:

1. *Gas–Gas.* There is gas on either side of $r = 0$. Based on the initial conditions, there are five possible resolutions for the gas–gas Riemann problem. It can be proven that the resolution to the Riemann problem with given initial conditions is unique in the class of centered shocks, rarefaction waves, and contact discontinuities separating constant states, if and only if

$$u_r - u_l < \frac{2}{\gamma - 1}(C_{gl}V_l + C_{gr}V_r). \tag{3.2}$$

Here C is the Lagrangian sound speed defined by

$$C^2 \equiv -\frac{\partial P}{\partial V} \tag{3.3}$$

and, accordingly,

$$C_g^2 = \frac{\gamma P}{V}, \quad C_w^2 = \frac{k\alpha p_a \rho_{\text{ref.}}{}^{\alpha-1}}{\rho_a^{\alpha} V^{\alpha+1}}, \tag{3.4}$$

where the subscript g stands for the gas and w for the water. If (3.2) is violated, a vacuum state will take place. Investigation shows that a vacuum can be bounded only by rarefaction waves. For details about the gas–gas Riemann problem; cf. [21, 12]. The Godunov scheme [15] and the MUSCL scheme [16] are based upon solutions without vacuum states to this Riemann problem.

Resolution 1. Under the restriction of (3.2), the solution to the gas–gas Riemann problem for (2.1) with (3.1) consists of four constant states connected by three centered waves (from the left to the right): a shock wave or a rarefaction wave, contact discontinuity, and a shock wave or a rarefaction wave. If the restriction is violated, the solution consists of a constant state, a rarefaction wave, a vacuum zone, a rarefaction wave, and a constant state.

2. *Water–Water.* Resolutions to this Riemann problem are somewhat different from those of above gas–gas Riemann problem. In the water–water Riemann problem, a resolution without a vacuum state has no contact discontinuity. When a vacuum takes place in the resolution, further difference may arise. If initial pressure on each side of $r = 0$ is positive, the vacuum will be located between two rarefaction waves. Nevertheless, if the initial pressure is negative, i.e., water can resist tensile stresses as indicated

in Section 2 ($p_v < 0$), this resolution should have a different pattern. The water phase located next to the vacuum has zero pressure and, since pressure at a rarefaction wave front should be higher than that at its tail, it cannot be connected with the initial water state with negative pressure by a centered rarefaction wave. Instead, it can be connected with the initial state by a centered shock wave. For this reason, we have to construct a new kind of resolution: a vacuum zone is located between two shocks. In the resolution, water pressure increases from negative to zero across a shock. The formulas of this newly constructed resolution are given in the following (3.19), and its wave system is different from each of the five possible resolved wave systems of the gas–gas Riemann problem. Consequently, if a resolution of the water–water Riemann problem has a vacuum zone, the vacuum zone lies either between rarefaction waves or between shocks. It should be noted that although the pressure on a water surface adjacent to a vacuum zone equals zero, density there is not zero. A (3.2)-like inequality is now given as

$$u_r - u_l < \frac{2}{\alpha - 1}(C_{wl}V_l + C_{wr}V_r) - \frac{4}{\alpha - 1}C_{wv}V_v. \quad (3.5)$$

The resolution of the initial discontinuity (3.1) now becomes

Resolution 2. If the condition of (3.5) is fulfilled, the solution to the water–water Riemann problem for (2.1) with (3.1) consists of three constant states connected by two centered waves: a shock wave or a rarefaction wave, and a shock wave or a rarefaction wave. If the condition is violated, it consists of a constant state, a shock wave or a rarefaction wave, a constant state with zero pressure, a vacuum zone, a constant state with zero pressure, a shock wave or a rarefaction wave, and a constant state.

3. *Gas–Water.* Gas and water are located on the left and right sides of $r = 0$, respectively. Consider an interface Γ separating gas and water. We use the system (2.1) to obtain Rankine–Hugoniot conditions,

$$W_\Gamma(V_- - V_+) + (u_- - u_+) = 0, \quad (3.6a)$$

$$W_\Gamma(u_- - u_+) - (P_- - P_+) = 0, \quad (3.6b)$$

$$W_\Gamma(E_- - E_+) - (u_-P_- - u_+P_+) = 0, \quad (3.6c)$$

where the subscripts $\pm$ represent the left and right sides of Γ, respectively, and W_Γ is the Lagrangian speed of the interface. Actually, $W_\Gamma = 0$ in that location of Γ remains the same in Lagrangian coordinate r. It is readily seen that

$$V_- > V_+, \quad u_- = u_+, \quad P_- = P_+ \quad (3.7)$$

satisfies (3.6), and this indicates that both velocity and pressure are continuous across the interface. It can be verified that Γ is a contact discontinuity defined by Lax [20]. The inequality

$$u_r - u_l < \frac{2}{\gamma - 1}C_{gl}V_l + \frac{2}{\alpha - 1}(C_{wr}V_r - C_{w0}V_0) \quad (3.8)$$

is a criterion, where the subscript 0 refers to zero pressure conditions.

Resolution 3. Under the condition of (3.8), the solution to the gas–water Riemann problem for (2.1) with (3.1) consists of four constant states connected by three centered waves: a shock wave or a rarefaction wave, a contact discontinuity, and a shock wave or a rarefaction wave. If (3.8) is not satisfied, it consists of a constant state, a rarefaction wave, a vacuum zone, a constant state with zero pressure, a shock wave or a rarefaction wave, and a constant state.

4. *Water or Gas–Vacuum.* Water or gas and a vacuum zone are located on the left and right side of $r = 0$, respectively. As we intend to develop a scheme for a flow with vacuums, the situation that initial conditions (3.1) contain a vacuum state has to be considered. A good discussion about the gas–vacuum Riemann problem was given by Liu and Smoller [12]. For the gas–vacuum Riemann problem, H_r is $(\infty, u_r, 0)$, in which u_r takes a value that enables H_r to be connected with H_l by a centered rarefaction wave. For the water–vacuum Riemann problem, we set H_r as $(V_0, u_r, 0)$. If $P_l \geq 0$ (or if initial water pressure is nonnegative), u_r is so chosen that H_r connects with H_l by a centered rarefaction wave. If $P_l < 0$ (or if initial pressure in water is negative), u_r is so chosen that H_r connects with H_l by a shock, and this is in agreement with the above newly constructed resolution.

Resolution 4. The solution to the Riemann problem for (2.1) with the initial conditions (3.1) that contain a vacuum zone consists of: (a) *water* ($P_l \geq 0$)–*vacuum*, a constant state, a rarefaction wave, a constant state with zero pressure, and a vacuum zone; (b) *water* ($P_l < 0$)–*vacuum*, a constant state, a shock wave, a constant state with zero pressure, and a vacuum zone; (c) *gas–vacuum*, a constant state, a rarefaction wave, and a vacuum zone.

According to the above discussions we now have

PROPOSITION 3.1. *The resolution of the Riemann problem for* (2.1) *with initial conditions* (3.1) *has four possible cases: Resolution* 1, *Resolution* 2, *Resolution* 3, *or Resolution* 4.

Resolutions 1–4 may contain vacuum states. For this reason, the method presented in this paper can describe the occurrence, development, and disappearance of cavitation

zones. The four resolutions are weak solutions to (2.1) and (3.1), and the formulas for these solutions will be given as follows.

3.2. *Solution to the Riemann Problem*

First, we consider the solution without a vacuum to the Riemann problem (2.1) and (3.1). R-H conditions in water give the relations between pre- and postshock physical variables as

$$\pm W_{\mathrm{w}}(V^* - V_s) + (u^* - u_s) = 0, \tag{3.9a}$$

$$\pm W_{\mathrm{w}}(u^* - u_s) - (P^* - P_s) = 0. \tag{3.9b}$$

Here the asterisks refer to postshock values, the subscript s stands for l or r, $\pm W_{\mathrm{w}}$ are the Langrangian shock speeds in water, the signs $\pm$ refer to the propagation direction of a wave, in this case the shock, (3.9) yields

$$u^* - u_s = \pm \frac{P^* - P_s}{W_{\mathrm{w}}}, \tag{3.10a}$$

$$W_{\mathrm{w}} = \sqrt{(P^* - P_s)(V_s - V^*)}. \tag{3.10b}$$

It follows from (3.10b) and (2.6) that

$$\lim_{P^* \to P_s + 0} W_{\mathrm{w}} = C_{\mathrm{w}s}. \tag{3.10c}$$

For a rarefaction wave in water, since the Riemann invariants of (2.1) are constant along characteristics, one has

$$u^* \pm \left(-\int \frac{c}{\rho} d\rho \right)^* = u_s \pm \left(-\int \frac{c}{\rho} d\rho \right)_s, \tag{3.11}$$

where c is the spatial sound speed defined by

$$c \equiv \sqrt{(\partial p / \partial \rho)_S} = CV, \tag{3.12}$$

in which capital S refers to the entropy. With the aid of (2.5), (3.11) may be written as

$$u^* - u_s = \pm \frac{2 V_s C_{\mathrm{w}s}}{\alpha - 1} \left(\frac{V^* C_{\mathrm{w}}^*}{V_s C_{\mathrm{w}s}} - 1 \right). \tag{3.13}$$

By virtue of jump conditions across a shock wave in gas, we obtain

$$u^* - u_s = \pm \frac{P^* - P_s}{W_{\mathrm{g}}}, \tag{3.14a}$$

$$W_{\mathrm{g}} = C_{\mathrm{g}s} \sqrt{[(\gamma + 1)P^* + (\gamma - 1)P_s]/2\gamma P_s}, \tag{3.14b}$$

$$\lim_{P^* \to P_s + 0} W_{\mathrm{g}} = C_{\mathrm{g}s}. \tag{3.14c}$$

For a rarefaction wave in gas, using (3.11) and the isentropic relation

$$\frac{P^*}{\rho^{*\gamma}} = \frac{P_s}{\rho_s^{\gamma}}, \tag{3.15}$$

we get

$$u^* - u_s = \pm \frac{2 V_s C_{\mathrm{g}s}}{\gamma - 1} \left(\left(\frac{P^*}{P_s} \right)^{(\gamma - 1)/2\gamma} - 1 \right). \tag{3.16}$$

Combining Eqs. (3.10a), (3.13), (3.14a), and (3.16), we have

$$u^* - u_s = \pm f(u_s, P_s, P^*), \tag{3.17a}$$

$$f(u_s, P_s, P^*) = \begin{cases} f_{\mathrm{w}}(u_s, P_s, P^*), & \text{in water,} \\ f_{\mathrm{g}}(u_s, P_s, P^*), & \text{in gas,} \end{cases} \tag{3.17b}$$

where

$$f_{\mathrm{w}}(u_s, P_s, P^*) = \begin{cases} \dfrac{2 V_s C_{\mathrm{w}s}}{\alpha - 1} \left(\dfrac{V^* C_{\mathrm{w}}^*}{V_s C_{\mathrm{w}s}} - 1 \right), & P_{\mathrm{v}} < P^* \le P_s, \\ \dfrac{P^* - P_s}{W_{\mathrm{w}}}, & P^* > P_s, \end{cases} \tag{3.17c}$$

$$f_{\mathrm{g}}(u_s, P_s, P^*) = \begin{cases} \dfrac{2 V_s C_{\mathrm{g}s}}{\gamma - 1} \left(\left(\dfrac{P^*}{P_s} \right)^{(\gamma - 1)/2\gamma} - 1 \right), & P_{\mathrm{v}} < P^* \le P_s, \\ \dfrac{P^* - P_s}{W_{\mathrm{g}}}, & P^* > P_s. \end{cases} \tag{3.17d}$$

Second, we turn to consider the solution with a vacuum to the Riemann problem for (2.1) with (3.1). For a water–vacuum Riemann problem, if water pressure is initially higher than zero, according to Resolution 4, there will be a rarefaction wave that propagates away from the vacuum. The resolved state behind the rarefaction wave is

$$\begin{aligned} V^* &= V_0, \\ u^* - u_s &= \pm \frac{2 V_s C_{\mathrm{w}s}}{\alpha - 1} \left(\frac{V_0 C_{\mathrm{w}0}}{V_s C_{\mathrm{w}s}} - 1 \right), \\ P^* &= 0. \end{aligned} \tag{3.18}$$

If that pressure is lower than zero, a shock wave will move away from the vacuum, and the postshock values are

$$V^* = V_0, \quad u^* - u_s = \pm\frac{-P_s}{W_{wv}}, \quad P^* = 0, \tag{3.19a}$$

$$W_{wv} = \sqrt{-P_s/(V_s - V_0)}. \tag{3.19b}$$

For a gas–vacuum Riemann problem, a rarefaction wave will propagate away from the vacuum, and at the tail of the rarefaction wave,

$$V^* = \infty, \quad u^* - u_s = \pm\frac{-2V_sC_{gs}}{\gamma - 1}, \quad P^* = 0. \tag{3.20}$$

3.3. *Existance and Uniqueness of the Solution for Riemann Problem*

Eliminating u^* from (3.17a) yields

$$f(u_l, P_l, P^*) + f(u_r, P_r, P^*) - (u_l - u_r) = 0. \tag{3.21}$$

We define

$$F_1(P) \equiv f(u_l, P_l, P) + f(u_r, P_r, P) - (u_l - u_r). \tag{3.22}$$

Whether there is a unique solution to (3.21) depends on whether $F_1(P)$ has a unique zero point or not. We will see that $F_1(P)$ is a monotonically increasing function passing through zero point once and only once, i.e., (3.21) has a unique solution.

It is known from (3.17) that

$$\lim_{P\to P_s^-0} f(u_s, P_s, P) = \lim_{P\to P_s^+0} f(u_s, P_s, P) = 0. \tag{3.23}$$

By some straightforward calculations we have

$$\frac{df_w(u_s, P_s, P)}{dP} = \begin{cases} \dfrac{1}{C_w}, & P_v < P \le P_s, \\ \dfrac{1}{2}\left(\dfrac{W_w}{C_w^2} + \dfrac{1}{W_w}\right), & P > P_s, \end{cases} \tag{3.24a}$$

$$\frac{df_g(u_s, P_s, P)}{dP} = \begin{cases} \dfrac{1}{C_{gs}}\left(\dfrac{P}{P_s}\right)^{-(\gamma+1)/2\gamma}, & P_v < P \le P_s. \\ \dfrac{W_g^2 + C_{gs}^2}{2W_g^3}, & P > P_s. \end{cases} \tag{3.24b}$$

It is easy to verify that

$$\lim_{P\to P_s^-0} \frac{df_w(u_s, P_s, P)}{dP} = \lim_{P\to P_s^+0} \frac{df_w(u_s, P_s, P)}{dP} = \frac{1}{C_{ws}}, \tag{3.24c}$$

$$\lim_{P\to P_s^-0} \frac{df_g(u_s, P_s, P)}{dP} = \lim_{P\to P_s^+0} \frac{df_g(u_s, P_s, P)}{dP} = \frac{1}{C_{gs}}. \tag{3.24d}$$

We may also have

$$\frac{d^2f_w(u_s, P_s, P)}{dP^2} = \tag{3.25a}$$

$$\begin{cases} -\dfrac{\alpha+1}{2VC_w^3}, & P_v < P \le P_s, \\ -\dfrac{\alpha+1}{2VW_wC_w^2}, & P > P_s, \end{cases}$$

$$\frac{d^2f_g(u_s, P_s, P)}{dP^2} = \tag{3.25b}$$

$$\begin{cases} -\dfrac{\gamma+1}{2V_sC_{gs}^3}\left(\dfrac{P}{P_s}\right)^{-(3\gamma+1)/2\gamma}, & P_v < P \le P_s. \\ -\dfrac{(\gamma+1)(W_g^2 + 3C_{gs}^2)}{8V_sW_g^5}, & P > P_s. \end{cases}$$

To obtain the second branch in (3.25a), we assume that $|V - V_s| \ll 1$, i.e., the change of water density is small. This assumption coincides with the premise for (2.5); (3.25) gives rise to

$$\lim_{P\to P_s^-0} \frac{d^2f_w(u_s, P_s, P)}{dP^2} \tag{3.25c}$$

$$= \lim_{P\to P_s^+0} \frac{d^2f_w(u_s, P_s, P)}{dP^2} = -\frac{\alpha+1}{2V_sC_{ws}^3},$$

$$\lim_{P\to P_s^-0} \frac{d^2f_g(u_s, P_s, P)}{dP^2} \tag{3.25d}$$

$$= \lim_{P\to P_s^+0} \frac{d^2f_g(u_s, P_s, P)}{dP^2} = -\frac{\gamma+1}{2V_sC_{gs}^3}.$$

Now we conclude from (3.22), (3.17), (3.23), (3.24), and (3.25) that

LEMMA 3.1. *$F_1(P)$ is a continuous and monotonically increasing function of P, both its first and second derivatives, remaining positive and negative, respectively, are also continuous.*

Equation (3.21) may be solved by the Newton method that is convergent of order 2, namely,

$$P^{(n+1)} = P^{(n)} - \left(\frac{F_1(P)}{dF_1(P)/dP}\right)^{(n)}, \tag{3.26a}$$

where

$$P^{(0)} = P_v \tag{3.26b}$$

or

$$P^{(0)} = \frac{P_l C_r + P_r C_l + (u_l - u_r) C_l C_r}{C_l + C_r}. \tag{3.26c}$$

Here the superscript (n) refers to the nth iteration.

THEOREM 3.1. (i) *In the class of centered shocks and rarefaction waves and contact discontinuities, the solution to the Riemann problem for* (2.1) *with* (3.1) *exists uniquely*;

(ii) *If the solution contains no vacuum, the iteration process* (3.26a) *with the initial value* (3.26b) *converges to the solution.*

Proof. (i). According to Proposition 3.1, the solution to the Riemann problem is a combination of centered shocks and rarefaction waves and contact discontinuities. First, consider the case that the solution contains no vacuum state. Let

$$F_2(P) \equiv f(u_l, P_l, P) + f(u_r, P_r, P). \tag{3.27}$$

Since there is no vacuum state, (3.2) or (3.5) or (3.8) holds, i.e., in terms of (3.27),

$$u_l - u_r > F_2(P_v) = \begin{cases} = 2(V_v C_{wv} - V_l C_{wl})/(\alpha - 1) & \\ \quad +2(V_v C_{wv} - V_r C_{wr})/(\alpha - 1), & \text{water–water,} \\ = -2V_l C_{gl}/(\gamma - 1) & \\ \quad +2(V_0 C_{w0} - V_r C_{wr})/(\alpha - 1), & \text{gas–water,} \\ = -2(V_l C_{gl} + V_r C_{gr})/(\gamma - 1), & \text{gas–gas.} \end{cases} \tag{3.28}$$

Because of (3.22) and (3.27), (3.28) gives rise to

$$F_1(P_v) < 0. \tag{3.29}$$

The definition of $F_1(P)$ yields

$$F_1(\infty) = \infty > 0. \tag{3.30}$$

By Lemma 3.1, it is known that $F_1(P)$ is a monotonically increasing function. As a result, $F_1(P)$ passes the zero point once and only once; i.e., there is always a unique P^* satisfying (3.21), hence a unique u^* and V^* that are explicitly given by (3.17) and some other formulas, herein $P^* \in (P_v, \infty)$. Therefore, in the case of having no vacuum, the solution to the Riemann problem exists uniquely.

Second, if there is a vacuum in the solution, P^*, u^*, and V^* are determined by (3.18)–(3.20). Consequently, the solution also exists uniquely.

(ii). Consider an interval (P_v, M), where M is a sufficiently large constant so that $F_1(M) > 0$ and $P^* \in (P_v, M)$. We conclude from (3.29), (3.30), and Lemma 3.1 that (1) $F_1(P_v)F_1(M) < 0$; (2) $dF_1(P)/dP \neq 0$; (3) $dF_1^2(P)/dP^2$ stays negative; and (4) $(F_1(P) \cdot dF_1^2(P)/dP^2)_{P=P_v} > 0$. It can be proven that the iteration (3.26a) with the initial value P_v will surely converge to its fixed point (see [22]):

$$\lim_{n\to\infty} P^{(n)} = P^*. \tag{3.31}$$

This completes the proof of Theorem 3.1. ∎

4. TIME DERIVATIVES FOR RESOLVED STATE

Consider the initial value problem for the system (2.1) with initial data

$$U_{t=0} = \begin{cases} Q_l(r), & r < 0, \\ Q_r(r), & r > 0. \end{cases} \tag{4.1}$$

Here $Q(r) = (V(r), u(r), P(r))$, each component of $Q_l(r)$ and $Q_r(r)$ is a linear function of r. The medium to the left and right of $r = 0$ may be water or gas, or may be a vacuum zone. The time derivatives $(\partial V/\partial t)^*$, $(\partial u/\partial t)^*$, and $(\partial P/\partial t)^*$ of the resolved state at $r = 0$ of the Riemann problem in the last section equal zero. But, this is no longer true in the gas–water–vacuum initial value problem for (2.1) with (4.1), and these time derivatives have to be determined.

We begin with the solution without a vacuum to the above initial value problem. Differentiating (3.9b) along the direction of $\pm W_w$ yields

$$\begin{aligned} \pm DW_w(u^* - u_s) \pm W_w((Du)^* - (Du)_s) \\ - (DP)^* + (DP)_s = 0, \end{aligned} \tag{4.2}$$

where $D = \partial/\partial t \pm W_w \partial/\partial r$, being a total differential operator. By the aid of (2.1) and (3.10b), it is derived from (4.2) that

$$\begin{aligned} &\left(\frac{W_w^3}{2C_w^{*2}} + \frac{3W_w}{2}\right)\left(\frac{\partial u}{\partial t}\right)^* \pm \left(-\frac{3W_w^2}{2C_w^{*2}} - \frac{1}{2}\right)\left(\frac{\partial P}{\partial t}\right)^* \\ &= \pm\left(\frac{3W_w^2}{2} + \frac{C_{ws}^2}{2}\right)\left(\frac{\partial u}{\partial r}\right)_s - \left(\frac{W_w^3}{2C_{ws}^2} + \frac{3W_w}{2}\right)\left(\frac{\partial P}{\partial r}\right)_s. \end{aligned} \tag{4.3}$$

Equation (4.3) is the formula for time derivatives of the resolved state behind a shock wave in water. For the case of a rarefaction wave in water, writing an equation in a

form similar to (3.9b),

$$\pm W_{\mathrm{wr}}(u^* - u_s) - (P^* - P_s) = 0, \tag{4.4a}$$

in which W_{wr} is defined as

$$W_{\mathrm{wr}} \equiv \frac{|P^* - P_s|}{|u^* - u_s|} = \frac{(\alpha - 1)(P^* - P_s)}{2(V^* C_{\mathrm{w}}^* - V_s C_{\mathrm{w}s})}, \tag{4.4b}$$

where

$$\lim_{P^* \to P_s - 0} W_{\mathrm{wr}} = C_{\mathrm{w}s}, \tag{4.4c}$$

we may also have

$$\left(\frac{W_{\mathrm{wr}}^2}{C_{\mathrm{w}}^*} + W_{\mathrm{wr}}\right)\left(\frac{\partial u}{\partial t}\right)^* \pm \left(-\frac{W_{\mathrm{wr}}}{C_{\mathrm{w}}^*} - \frac{W_{\mathrm{wr}}^2}{C_{\mathrm{w}s}^2}\right)\left(\frac{\partial P}{\partial t}\right)^* = \pm(W_{\mathrm{wr}}^2 + C_{\mathrm{w}s} W_{\mathrm{wr}})\left(\frac{\partial u}{\partial r}\right)_s - \left(\frac{W_{\mathrm{wr}}^2}{C_{\mathrm{w}s}} + W_{\mathrm{wr}}\right)\left(\frac{\partial P}{\partial r}\right)_s. \tag{4.5}$$

In a gas flow, we obtain

$$\begin{aligned}
&\left(\frac{(\gamma+1) W_{\mathrm{g}}(V^* - V_s)}{4V_s} + 2W_{\mathrm{g}}\right)\left(\frac{\partial u}{\partial t}\right)^* \\
&\pm\left(-\frac{W_{\mathrm{g}}^2}{C_{\mathrm{g}}^{*2}} - \frac{(\gamma+1)(V^* - V_s)}{4V_s} - 1\right)\left(\frac{\partial P}{\partial t}\right)^* \\
&= \pm\left(-\frac{W_{\mathrm{g}}^2(V^* - V_s)}{2V_s} - \frac{(\gamma-1) C_{\mathrm{g}s}^2 (V^* - V_s)}{4V_s} + W_{\mathrm{g}}^2 + C_{\mathrm{g}s}^2\right)\left(\frac{\partial u}{\partial r}\right)_{\mathrm{s}} \\
&\quad + \left(\frac{(\gamma-1) W_{\mathrm{g}}(V^* - V_s)}{4V_s} + \frac{W_{\mathrm{g}}^3 (V^* - V_s)}{2V_s C_{\mathrm{g}s}^2} - 2W_{\mathrm{g}}\right)\left(\frac{\partial P}{\partial r}\right)_s
\end{aligned} \tag{4.6}$$

for the time derivatives behind a shock wave and

$$\begin{aligned}
&\left(\frac{W_{\mathrm{gr}}^2}{C_{\mathrm{g}}^*} + W_{\mathrm{gr}}\right)\left(\frac{\partial u}{\partial t}\right)^* \pm \left(-\frac{W_{\mathrm{gr}}}{C_{\mathrm{g}}^*} - \frac{W_{\mathrm{gr}}^2}{C_{\mathrm{g}s}^2}\right)\left(\frac{\partial P}{\partial t}\right)^* \\
&= \pm\left(-\left(1 - \frac{W_{\mathrm{gr}}}{C_{\mathrm{g}}^*}\right)\frac{\mathbf{C}_{\mathrm{g}s}^2 P^*}{P_s} + \frac{(\gamma+1)(P^* - P_s)}{2V_s} + W_{\mathrm{gr}}^2 + C_{\mathrm{g}s}^2\right)\left(\frac{\partial u}{\partial r}\right)_s \\
&\quad + \left(\left(1 - \frac{W_{\mathrm{gr}}}{C_{\mathrm{g}}^*}\right)\frac{W_{\mathrm{gr}} P^*}{P_s} - \frac{(\gamma+1) W_{\mathrm{gr}}(P^* - P_s)}{2V_s C_{\mathrm{g}s}^2} - 2W_{\mathrm{gr}}\right)\left(\frac{\partial P}{\partial r}\right)_s
\end{aligned} \tag{4.7a}$$

for the time derivatives behind a rarefaction wave. Here

$$W_{\mathrm{gr}} \equiv \frac{|P^* - P_s|}{|u^* - u_s|} = \frac{(\gamma-1) P_s^{(\gamma-1)/2\gamma}(P^* - P_s)}{2V_s C_{\mathrm{g}s}(P^{*(\gamma-1)/2\gamma} - P_s^{(\gamma-1)/2\gamma})}, \tag{4.7b}$$

$$\lim_{P^* \to P_s - 0} W_{\mathrm{gr}} = C_{\mathrm{g}s}. \tag{4.7c}$$

(4.6) and (4.7a) are different from those obtained by van Leer [16] under the restriction of $|C_{\mathrm{g}s} - C_{\mathrm{g}}^*| \ll 1$. In our deduction the restriction is not imposed and no term has been neglected.

Two formulas among (4.3) and (4.5)–(4.7a), one for a wave facing the right and the other for that facing the left, comprise the following linear algebraic system for time derivatives at $r = 0$ resulting immediately after resolution of the initial discontinuity (4.1),

$$\begin{pmatrix} a_{11} & -a_{12} \\ a_{21} & a_{22} \end{pmatrix}\begin{pmatrix} \left(\frac{\partial u}{\partial t}\right)^* \\ \left(\frac{\partial P}{\partial t}\right)^* \end{pmatrix} = \begin{pmatrix} b_1 \\ b_2 \end{pmatrix}, \tag{4.8a}$$

where

$$a_{11}, a_{21} = \begin{cases} W_{\mathrm{w}}^3/(2C_{\mathrm{w}}^{*2}) + 3W_{\mathrm{w}}/2, & \text{shock in water,} \\ W_{\mathrm{wr}}^2/C_{\mathrm{w}}^* + W_{\mathrm{wr}}, & \text{rarefaction wave in water,} \\ (\gamma+1) W_{\mathrm{g}}(V^* - V_s)/(4V_s) + 2W_{\mathrm{g}}, & \text{shock in gas,} \\ W_{\mathrm{gr}}^2/C_{\mathrm{g}}^* + W_{\mathrm{gr}}, & \text{rarefaction wave in gas,} \end{cases} \tag{4.8b}$$

$$a_{12}, a_{22} = \begin{cases} 3W_{\mathrm{w}}^2/(2C_{\mathrm{w}}^{*2}) + 1/2, & \text{shock in water,} \\ W_{\mathrm{wr}}/C_{\mathrm{w}}^{*} + W_{\mathrm{wr}}^2/C_{\mathrm{w}s}^2, & \text{rarefaction wave in water,} \\ W_{\mathrm{g}}^2/C_{\mathrm{g}}^{*2} + (\gamma+1)(V^{*} - V_s)/(4V_s) + 1, & \text{shock in gas,} \\ W_{\mathrm{gr}}/C_{\mathrm{g}}^{*} + W_{\mathrm{gr}}^2/C_{\mathrm{g}s}^2, & \text{rarefaction wave in gas,} \end{cases} \tag{4.8c}$$

and b_1, b_2 are linear functions of $(\partial u/\partial t)_s$ and $(\partial P/\partial t)_s$. Noticing (3.10c), (3.14c), (4.4c), and (4.7c), it is not difficult to verify that $a_{k,m} > 0$ $(k, m = 1, 2)$ in case of $\gamma \le 3$. Then

$$\mathrm{DET}(a_{k,m}) = a_{11}a_{22} + a_{12}a_{21} > 0. \tag{4.9}$$

On the basis of linear algebra, (4.9) gives the following results.

ASSERTION 3.1. *Under the restriction of* $\gamma \le 3$, *the solution of* (4.8a) *exists uniquely.*

If $(\partial u/\partial t)_s = (\partial P/\partial t)_s = 0$, then $b_1 = b_2 = 0$ and $(\partial u/\partial t)^* = (\partial P/\partial t)^* = 0$. This situation corresponds to the case of the first-order Godunov scheme. On determining $(\partial P/\partial t)^*$, $(\partial V/\partial t)^*$ is given as

$$\left(\frac{\partial V}{\partial t}\right)^* = \frac{1}{C^{*2}}\left(\frac{\partial P}{\partial t}\right)^*. \tag{4.10}$$

We now consider the solution with a vacuum state to the initial value problem for (2.1) with (4.1). Since density keeps constant and pressure is always zero on a gas or water surface adjoining a vacuum, we have

$$\left(\frac{\partial V}{\partial t}\right)^* = \left(\frac{\partial P}{\partial t}\right)^* = 0. \tag{4.11}$$

But, velocity there may change with time. If pressure is initially higher than zero on a water surface adjacent to a vacuum, it follows from (3.18) that

$$\left(\frac{W_{\mathrm{wrv}}^2}{2C_{\mathrm{w0}}^2} + W_{\mathrm{wrv}}\right)\left(\frac{\partial u}{\partial t}\right)^* = \pm(C_{\mathrm{w}s}W_{\mathrm{wrv}} + W_{\mathrm{wrv}}^2)\left(\frac{\partial u}{\partial r}\right)_s - \left(W_{\mathrm{wrv}} + \frac{W_{\mathrm{wrv}}^2}{C_{\mathrm{w}s}}\right)\left(\frac{\partial P}{\partial r}\right)_s, \tag{4.12a}$$

$$W_{\mathrm{wrv}} \equiv \frac{|P_s|}{|u^* - u_s|} = \frac{(\alpha-1)(-P_s)}{2(V_0C_{\mathrm{w0}} - V_sC_{\mathrm{w}s})}. \tag{4.12b}$$

If the pressure is lower than zero, (3.19a) holds and it gives

$$\left(\frac{W_{\mathrm{wv}}^3}{2C_{\mathrm{w0}}^2} + \frac{3W_{\mathrm{wv}}}{2}\right)\left(\frac{\partial u}{\partial t}\right)^* = \pm\left(\frac{3W_{\mathrm{wv}}^2}{2} + \frac{C_{\mathrm{w}s}^2}{2}\right)\left(\frac{\partial u}{\partial r}\right)_s - \left(\frac{W_{\mathrm{wv}}^3}{2C_{\mathrm{w}s}^2} + \frac{3W_{\mathrm{wv}}}{2}\right)\left(\frac{\partial P}{\partial r}\right)_s. \tag{4.13}$$

At the tail of a rarefaction wave by which a gas constant state is connected with a vacuum, (3.20) gives

$$\left(\frac{\partial u}{\partial t}\right)^* = \pm\frac{(3\gamma-1)C_{\mathrm{g}s}}{2\gamma}\left(\frac{\partial u}{\partial r}\right)_s - \frac{3\gamma-1}{2\gamma}\left(\frac{\partial P}{\partial r}\right)_s. \tag{4.14}$$

5. E-MUSCL SCHEME

Consider a fluid slab (r_i, r_{i+1}) in which V, u, and P are smooth. Integrating the first equation in (2.1) over the slab and a time step with the use of Green formula results in

$$\int_{r_i}^{r_{i+1}} V^{n+1}dr = \int_{r_i}^{r_{i+1}} V^n dr + \int_{t^n}^{t^{n+1}} u^*_{(i+1)-}dt - \int_{t^n}^{t^{n+1}} u^*_{i+}\,dt. \tag{5.1}$$

In the slab, V is approximated by a linear distribution

$$V_{\mathrm{approx.}} = \overline{V}_{i+1/2} + \frac{\Delta_{i+1/2}V}{\Delta_{i+1/2}r}(r - r_{i+1/2}), \quad r_i < r < r_{i+1}, \tag{5.2a}$$

where

$$\overline{V}_{i+1/2} \equiv \frac{1}{\Delta_{i+1/2}r}\int_{r_i}^{r_{i+1}} V_{\mathrm{approx.}}\,dr, \tag{5.2b}$$

and $r_{i+1/2} = (r_{i+1} + r_i)/2$, $\Delta_{i+1/2}r = r_{i+1} - r_i$, $\Delta_{i+1/2}V = V^*_{(i+1)-} - V^*_{i+}$. $\Delta_{i+1/2}V$ is the slope of V in the slab. It

follows from (5.1) that

$$\overline{V}_{i+1/2}^{n+1} = \overline{V}_{i+1/2}^{n} + \lambda_{i+1/2}^{n+1/2}(\langle u\rangle_{(i+1)-} - \langle u\rangle_{i+}) + O((\Delta^{n+1/2}t)^3, \Delta^{n+1/2}t(\Delta_{i+1/2}r)^2), \tag{5.3a}$$

where

$$\langle u\rangle = u^{*n} + \frac{1}{2}\left(\frac{\partial u}{\partial t}\right)^{*n}\Delta^{n+1/2}t, \tag{5.3b}$$

$\lambda_{i+1/2}^{n+1/2} = \Delta^{n+1/2}t/\Delta_{i+1/2}r$, and $\Delta^{n+1/2}t = t^{n+1} - t^n$, being the time step at t^n. Omitting higher order terms in (5.3a), it is obtained that

$$\overline{V}_{i+1/2}^{n+1} = \overline{V}_{i+1/2}^{n} + \lambda_{i+1/2}^{n+1/2}(\langle u\rangle_{(i+1)-} - \langle u\rangle_{i+}). \tag{5.4}$$

Similarly, the followings are obtained by using the other two equations in (2.1),

$$\overline{u}_{i+1/2}^{n+1} = \overline{u}_{i+1/2}^{n} - \lambda_{i+1/2}^{n+1/2}(\langle P\rangle_{(i+1)-} - \langle P\rangle_{i+}), \tag{5.5}$$

$$\overline{E}_{i+1/2}^{n+1} = \overline{E}_{i+1/2}^{n} - \lambda_{i+1/2}^{n+1/2}(\langle u\rangle_{(i+1)-}\langle P\rangle_{(i+1)-} - \langle u\rangle_{i+}\langle P\rangle_{i+}), \tag{5.6}$$

where each notation stands for a meaning similar to that given in (5.4).

In ideal gas

$$P = \frac{\gamma - 1}{V}\left(E - \frac{u^2}{2}\right). \tag{5.7a}$$

Integrating (5.7a) and (2.6) and then omitting higher order terms, we obtain for the gas phase the sufficiently accurate formula

$$\overline{P}_{i+1/2} = \frac{\gamma - 1}{\overline{V}_{i+1/2}}\left(\overline{E}_{i+1/2} - \frac{\overline{u}_{i+1/2}^2}{2}\right), \tag{5.7b}$$

and for the water phase,

$$\overline{P}_{i+1/2} = \begin{cases} \dfrac{p_a}{\rho_{\text{ref.}}}\left(k\left(\left(\dfrac{\rho_{\text{ref.}}}{\rho_a \overline{V}_{i+1/2}}\right)^{\alpha} - 1\right) + 1\right), & \overline{V}_{i+1/2} < V_{\text{v}}, \\ 0, & \overline{V}_{i+1/2} \geq V_{\text{v}}. \end{cases} \tag{5.8}$$

Here $\overline{P}_{i+1/2}$ is defined similarly as $\overline{V}_{i+1/2}$.

We assume that vacuums may and only may appear between slabs. Since it is impossible to describe vacuum zones only in a Lagrangian reference frame, we have to track them in Eulerian coordinates. A vacuum zone at r_i is confined between its left end x_{i-} and right end x_{i+}, which are approximated in third-order accuracy by

$$x_{i-}^{n+1} = x_{i-}^{n} + \langle u\rangle_{i-}\Delta^{n+1/2}t, \quad x_{i+}^{n+1} = x_{i+}^{n} + \langle u\rangle_{i+}\Delta^{n+1/2}t. \tag{5.9}$$

Equations (5.9) can also track a gas–water interface.

In computations, (5.4), (5.5), and (5.8) are used for the water phase; (5.4), (5.5), (5.6), and (5.7b) are adopted for the gas phase; while (5.9) is employed to track vacuum zones. We call (5.4)–(5.7b), (5.8), and (5.9) the E-MUSCL scheme. This scheme is second-order accurate in view of margins of the third-order terms omitted in (5.4)–(5.6). Its accuracy may be affected by a slope limitation, such as a monotonicity algorithm in [16] or the algorithm for lower bound of density (6.9) in the next section. The proposed scheme becomes the first-order accurate Godunov scheme if all slab slopes are set equal to zero. Equations (5.4)–(5.6) are similar to the formulas of the Lagrangian steps in the standard MUSCL scheme [16]. However, on the basis of the initial value problems discussed in the previous sections, other than a flow for a gas continuum, (5.4)–(5.6) are also applicable to a gas–water–vacuum flow. Accordingly, the E-MUSCL scheme presented in this paper contains the standard MUSCL as a special case.

If a vacuum takes place at r_i, x_{i-} and x_{i+} will take different values, and they are given by (5.9). If $x_{i-} \neq x_{i+}$, the resolution of an initial discontinuity at r_i will belong to Resolution 4 stated in Section 3. When x_{i-} and x_{i+} become the same (when $|x_{i+} - x_{i-}| \leq \varepsilon$ in practical calculations, ε being positive and sufficiently small), the vacuum at r_i vanishes, and the resolution will belong to one of the other three resolutions. Hence, accuracy of the procedure to track vacuum zones may affect the accuracy of (5.4)–(5.6). If there is no vacuum state, summations $\sum_i \Delta_{i+1/2}r\overline{V}_{i+1/2}^n$, $\sum_i \Delta_{i+1/2}r\overline{u}_{i+1/2}^n$, and $\sum_i \Delta_{i+1/2}r\overline{E}_{i+1/2}^n$ are conserved exactly by (5.4)–(5.6), except for the fluxes at boundaries. But for a flow with vacuums, $\sum_i \Delta_{i+1/2}r\overline{V}_{i+1/2}^n$ may not be conserved, since $\langle u\rangle_{i-}$ and $\langle u\rangle_{i+}$ are not necessarily the same and, thus, they do not cancel each other in summing up (5.4). Actually, $\sum_i \Delta_{i+1/2}r\overline{V}_{i+1/2}^n$ is an approximation of $\int_{r_{1+}}^{r_{i_{\max}-}} V\,dr$, which, in view of (2.3), equals $\sum_i (x_{(i+1)-} - x_{i+})$, the total length occupied by fluids. Due to (5.1) and the fact that u_i^* can be different from u_{i+}^* when there is a vacuum at r_i, $\int_{r_{1+}}^{r_{i_{\max}-}} V\,dr$ may change with time. In the presence of vacuums the other two summations are still conserved, because $\langle P\rangle_{i-} = \langle P\rangle_{i+} = 0$ whenever a vacuum state occurs at r_i.

In order to suppress numerical oscillations, we employ the limiting technique (101) given in [16]. This technique requires the linear distribution of a state quantity in a slab not taking values beyond the average value in its

neighboring cells, and a slope is set equal to zero if its slab average is an extremum with respect to its neighboring averages. Our computations show that the technique is useful to enable the calculations to go forward, since the density slope of a water slab, which is usually located near a shock wave, may be so steep that pressure given by (2.6) becomes a large number and, thus, leads the computations to overflow.

For the sake of stability, no waves issuing from two ends of a slab are allowed to interact with each other; thus one has

$$\Delta^{n+1/2}t \le \frac{\mathrm{CFL}\Delta_{i+1/2}r}{2\mathrm{Max}(|W_{i+}|, |W_{(i+1)-}|)}, \tag{5.10a}$$

where W_i is the speed of either a shock wave or a rarefaction wave front, and CFL ≤ 1, noting that CFL may be larger than 1 in computations. The following restriction is imposed to avoid zone-tangling, i.e., the left end of a slab is not allowed to move across its right end, or vice versa,

$$\Delta^{n+1/2}t \le -\frac{\Delta^n_{i+1/2}x}{\Delta^n_{i+1/2}u}, \tag{5.10b}$$

where $\Delta^n_{i+1/2}u = u^n_{(i+1)-} - n^n_{i+} < 0$ and $\Delta^n_{i+1/2}x = x^n_{(i+1)-} - x^n_{i+}$. In the presence of vacuums, it is also necessary to avoid slab overlapping; i.e., it is required that $x_{i+} - x_{i-} \ge 0$. For this purpose, making use of (5.9) and omitting second-order terms, we give another restriction on the time step ($u^{*n}_{i-} > u^{*n}_{i+}$):

$$\Delta^{n+1/2}t \le \frac{x^n_{i+} - x^n_{i-}}{u^{*n}_{i-} - u^{*n}_{i+}}. \tag{5.10c}$$

The algorithm for lower bound of density given in inequality (6.10) or (6.11b) in the next section will be the additional set of restriction on the time step.

6. ALGORITHMS FOR LOWER BOUND OF DENSITY

In computations, we require not only $\overline{V}^{n+1}_{i+1/2} > 0$, but also

$$\overline{V}^{n+1}_{i+1/2} < V_{\mathrm{v}}, \tag{6.1}$$

which is equivalent to

$$\frac{\rho_{\mathrm{ref.}}}{\overline{V}^{n+1}_{i+1/2}} > \rho_{\mathrm{v}}, \tag{6.2}$$

where $\rho_{\mathrm{ref.}}/\overline{V}^{n+1}_{i+1/2}$ may be considered as the computed density. From the cavitation model described in Section 2, it is known that ρ_{v} is the lowest density of a fluid. Therefore, (6.1) requires that the computed density not be smaller than ρ_{v}. Inequality (6.1) always holds for gas, since $V_{\mathrm{v}} = +\infty$ in gas, whereas this is not true for water. $\overline{P}^{n+1}_{i+1/2}$ given by (5.8) will be much lower than p_{v} if $\overline{V}^{n+1}_{i+1/2}$ is slightly higher than V_{v}. This may cause severe numerical errors when cavitation lasts for a time comparable to the characteristic time of the computed flow. To calculate accurately a flow with cavitation zones, the requirement (6.1) should be satisfied. But, can it be fulfilled by the E-MUSCLE scheme?

LEMMA 6.1. *A sufficient condition for* (6.1) *is*

$$\lambda^{n+1/2}_{i+1/2}(\langle u\rangle_{(i+1)-} - \langle u\rangle_{i+}) < V_{\mathrm{v}} - \overline{V}^n_{i+1/2}. \tag{6.3}$$

Proof. Making use of (5.4), the proof is obvious. ▮

If $0 < \overline{V}^n_{i+1/2} < V_{\mathrm{v}}$, (6.3) is true for $\langle u\rangle_{(i+1)-} - \langle u\rangle_{i+} < 0$, which relates to compression of the cell (r_{i+1}, r_{i+1}) and appears generally as a flow becomes condensed. But, its violation is possible for $\langle u\rangle_{(i+1)-} - \langle u\rangle_{i+} > 0$, which corresponds to expansion of the cell and usually happens when a flow is rarefied.

THEOREM 6.1. *Suppose*

$$\left|\left(\frac{\partial u}{\partial t}\right)^{*n}_{(i+1)-} - \left(\frac{\partial u}{\partial t}\right)^{*n}_{i+}\right| < M\Delta_{i+1/2}r, \tag{6.4a}$$

$M = \mathrm{const} \ge 0$. *Then*, (6.1) *holds*, *provided*

$$\lambda^{n+1/2}_{i+1/2}\Delta^n_{i+1/2}u < V_{\mathrm{v}} - \overline{V}^n_{i+1/2} - \frac{M}{2}(\Delta^{n+1/2}t)^2. \tag{6.4b}$$

Proof. It follows form (5.4), (6.4a), and (6.4b) that

$$\begin{aligned}\lambda^{n+1/2}_{i+1/2}(\langle u\rangle_{i+1} - \langle u\rangle_i) &< \lambda^{n+1/2}_{i+1/2}\Delta^n_{i+1/2}u + \frac{M}{2}(\Delta^{n+1/2}t)^2 \\ &< V_{\mathrm{v}} - \overline{V}^n_{i+1/2},\end{aligned} \tag{6.4c}$$

which turns out to be (6.3). Then (6.1) follows from Lemma 6.1. ▮

ASSERTION 6.1. *If* (6.4b) *holds*, *then*

$$\lambda^{n+1/2}_{i+1/2}\Delta^n_{i+1/2}u < V_{\mathrm{v}} - \overline{V}^n_{i+1/2}. \tag{6.5}$$

In order to keep density higher than its minimum bound, some limiters will be constructed as follows. Consider a water particle in a slab (r_i, r_{i+1}) within which the density is smooth. Let the particle density be ρ^n at time t^n. Assume its density has decreased at time t^{n+1} but still remains higher

than ρ_v, then

$$\rho^{n+1} = \rho^n + \left(\frac{\partial \rho}{\partial t}\right)^n \Delta^{n+1/2} t + O((\Delta^{n+1/2} t)^2) > \rho_v. \quad (6.6)$$

Using (5.4) and the first equation in (2.1) and omitting higher order terms, we have

$$\lambda_{i+1/2}^{n+1/2} \Delta_{i+1/2}^n u < \overline{V}_{i+1/2}^n \left(1 - \frac{\overline{V}_{i+1/2}^n}{V_v}\right). \quad (6.7)$$

Inequality (6.7) can guarantee the validity of (6.5), that is,

THEOREM 6.2. *Let* $0 < \overline{V}_{i+1/2}^n < V_v$. *If* (6.7) *is satisfied, then* (6.5) *holds.*

Proof. It follows from (6.7) and the given condition of $0 < \overline{V}_{i+1/2}^n < V_v$ that

$$\begin{aligned} \lambda_{i+1/2}^{n+1/2} \Delta_{i+1/2}^n u &< \overline{V}_{i+1/2}^n \left(1 - \frac{\overline{V}_{i+1/2}^n}{V_v}\right) \\ &= \frac{\overline{V}_{i+1/2}^n}{V_v} \left(V_v - \overline{V}_{i+1/2}^n\right) \\ &< V_v - \overline{V}_{i+1/2}^n, \end{aligned} \quad (6.8)$$

this completes the proof of the theorem. ∎

Inequality (6.7) may be satisfied in two ways. The first way is to adjust the velocity slope of each slab. Since in the E-MUSCL procedure $\Delta^{n+1/2} t$ relates to $\Delta_{i+1/2}^n u$ by (5.10b) and (5.10c), solving (6.7) needs iterations. To make it simple, we replace $\Delta^{n+1/2} t$ by $\Delta^{n-1/2} t$. Then, velocity slope $\Delta_{i+1/2}^n u$ resulting from the E-MUSCL procedure is modified by the limiter

$$\begin{aligned} (\Delta_{i+1/2}^n u)_{\text{low1}} = \text{Min}\Bigg(&\Delta_{i+1/2}^n u, \overline{V}_{i+1/2}^n \\ &\left(1 - \frac{\overline{V}_{i+1/2}^n}{V_v}\right) \frac{\Delta_{i+1/2} r}{\Delta^{n-1/2} t}\Bigg). \end{aligned} \quad (6.9)$$

The other way is to restrict the time step,

$$\begin{aligned} (\Delta^{n+1/2} t)_{\text{low2}} = \text{Min}\Bigg(&\Delta^{n+1/2} t, \overline{V}_{i+1/2}^n \\ &\left(1 - \frac{\overline{V}_{i+1/2}^n}{V_v}\right) \frac{\Delta_{i+1/2} r}{\Delta_{i+1/2}^n u}\Bigg), \end{aligned} \quad (6.10)$$

where $\Delta_{i+1/2}^n u > 0$, and $\Delta^{n+1/2} t$ is determined by (5.10).

One more limiter can be derived from (6.6). For a resolution of an initial discontinuity at r_i, by using (6.6) and neglecting higher order terms, it is obtained that

$$\left(\frac{\partial V}{\partial t}\right)_{i\pm}^{*n} \Delta^{n+1/2} t < V_{i\pm}^{*n} \left(1 - \frac{V_{i\pm}^{*n}}{V_v}\right). \quad (6.11a)$$

We now have

$$(\Delta^{n+1/2} t)_{\text{low3}} = \text{Min}\left(\Delta^{n+1/2} t, \frac{V_{i\pm}^{*n}(1 - V_{i\pm}^{*n}/V_v)}{(\partial V/\partial t)_{i\pm}^{*n}}\right), \quad (6.11b)$$

in which $(\partial V/\partial t)_{i\pm}^{*n}$ are positive and determined by (4.10), and $\Delta^{n+1/2} t$ is evaluated according to (5.10).

We call (6.9), (6.10), and (6.11b) the algorithms for lower bound of density. Their effectiveness will be tested by numerical experiments presented in Section 7. Theorem 6.2 suggests that (6.7) is a little more stringent than (6.5). Thus, the algorithms (6.9) and (6.10) may lead to (6.4b) and, under the assumption of (6.4a), then to (6.1). We also have the following results about an expanding gas flow.

THEOREM 6.3. *Suppose that u and P are sufficiently smooth within gas slabs. Further assume that* $\langle u \rangle_{(i+1)-} - \langle u \rangle_{i+}$, $\overline{V}_{i+1/2}^n, P_{i+}^{*n} + P_{(i+1)-}^{*n} > 0$. *Then the E-MUSCL scheme gives*

$$\overline{P}_{i+1/2}^{n+1} > 0, \quad (6.12a)$$

provided

$$\Delta_{i+1/2}^n u < \frac{(\gamma - 1)\overline{V}_{i+1/2}^n \overline{P}_{i+1/2}^n}{\lambda_{i+1/2}^{n+1/2}(P_{i+}^{*n} + P_{(i+1)-}^{*n})}. \quad (6.12b)$$

Theorem 6.3 can be proven with the aid of (5.4)–(5.6). This theorem states that in the simulation of a gas flow from rarefied to vacuum state, to limit velocity slopes is also helpful for preventing the pressure updated by the E-MUSCL scheme from becoming negative.

7. NUMERICAL EXAMPLES

7.1. *Application to Gas–Water Riemman Problem*

To illustrate the performance of the method described in this paper, we first compute the gas–water Riemann problem

$$U_{t=0} = \begin{cases} G_l, & x < 0, \\ G_r, & x > 0, \end{cases} \quad (7.1)$$

where $G = (\rho, u, p)$. At initial time, the gas and the water

are located to the left and right of $x = 0$, respectively. There are six possible resolved wave systems for the gas–water Riemann problem. Here we show the numerical results of four wave systems whose initial conditions are respectively

$$U_{t=0} = \begin{cases} (50, 8, 4053000), & x < 0, \\ (1000.41282, 5, 1013250), & x > 0, \end{cases} \quad (7.2a)$$

$$U_{t=0} = \begin{cases} (50, 1000, 10132500), & x < 0, \\ (1002.23517, -100, 5066250), & x > 0, \end{cases} \quad (7.2b)$$

$$U_{t=0} = \begin{cases} (20, -1000, 5066250), & x < 0, \\ (1002.23517, 1000, 5066250), & x > 0, \end{cases} \quad (7.2c)$$

$$U_{t=0} = \begin{cases} (20, -1000, 5066250), & x < 0, \\ (997.64046, 1000, -5066250), & x > 0, \end{cases} \quad (7.2d)$$

where ρ, u, and $p_v = 0$ are respectively in kg/m^3, m/s, and Pa. (7.2c) results in two rarefaction waves moving in opposite directions and a vacuum zone in-between, and the resolution of (7.2d) contains a rarefaction wave, a vacuum, and a shock wave across which pressure increases from negative to zero.

In Figs. 1–6, the numerical values are shown by diamonds, and the exact solutions are shown by the solid lines. Numerical solutions for ρ, u, and p depicted in Fig. 1 agree well with exact solutions. As indicated in Fig. 2, the computed shocks in gas and water are confined to a narrow band of about two mesh cells, essentially without oscillations pre- and postshock waves. In Figs. 3 and 4, numerical accuracy for rarefaction waves in both water and gas is satisfactory, and vacuum zones are well resolved. The numerical results with the Godunov scheme, attained by setting all slab slopes equal to zero in the E-MUSCL code, are also given in Figs. 5 and 6. Compared with the results in Figs. 2, 3, 5, and 6, it is seen that the E-MUSCL scheme gives better approximations. In the computations, $\gamma = 2$, CFL = 1, $p_v = 0$, and there are 50 cells in gas and 50 cells in water, respectively, with an equal grid spacing.

7.2. *Prediction of the Flow in Water Shock Tube*

The water shock tube is a steel tube with its two ends sealed. The tube is filled with water, and a small piece of dynamite is placed at its center. At each end of the tube a sensor for measuring the explosion pressure is installed, one being the standard and the other being that to be

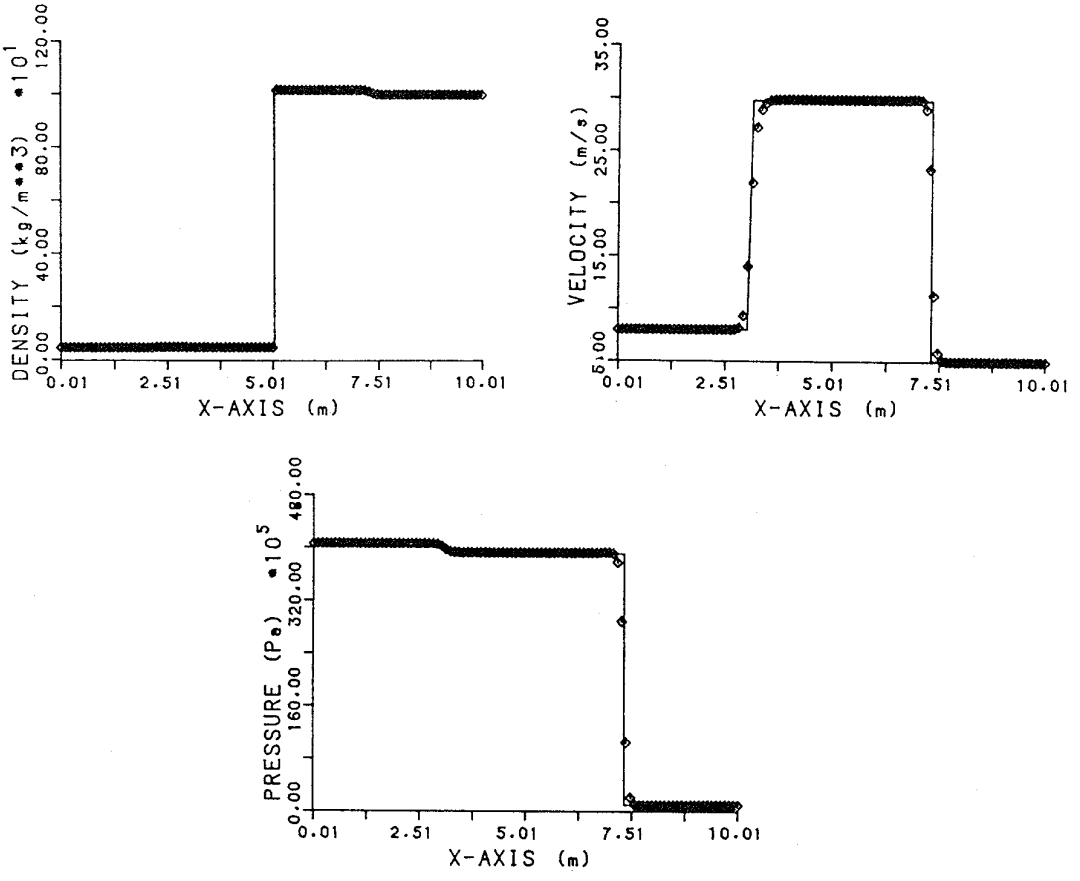

FIG. 1. Solutions for (7.2a) at $t = 0.00151$.

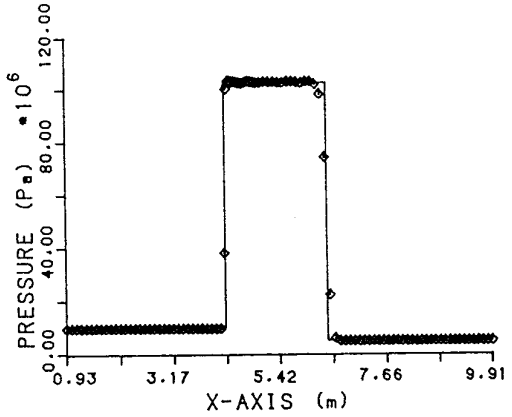

FIG. 2. Solutions for (7.2b) at $t = 0.00093$.

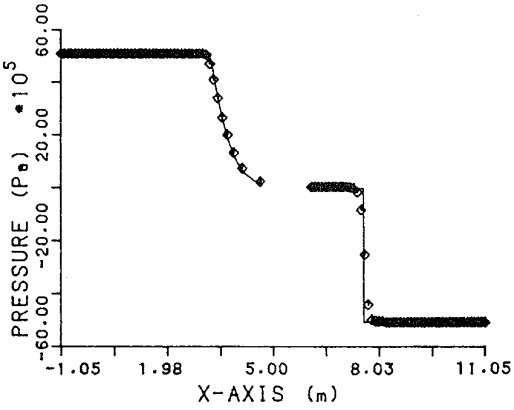

FIG. 4. Solutions for (7.2d) at $t = 0.00105$. A vacuum appears between gas and water.

calibrated. It is expected that pressure at the end might behave similarly to that at a wall where a shock in the air reflects; i.e., it rises suddenly when the blast wave reaches the end and then decays smoothly with time. However, as depicted in Fig. 7, experiments indicate clearly that the end pressure decreases with a pattern of multiple jumps and drops (the solid line) rather than in a smooth fashion (the dotted line). Even if an initial pressure of about 200 atm is exerted in the water befor explosion, the jumps and drops could not be eliminated, and the end pressure would decrease to a value lower than the initial pressure (see [8]).

The flow in the water shock tube is rather complicated. To study the early stage of the flow, which lasts for as short as milliseconds, we assume that: (1) *there is an interface with no Taylor instability between the water and the gaseous products of the dynamite, and both of them are initially at rest*; (2) *the flow is one-dimensional and symmetrical about the tube center*; (3) *there is no viscosity and heat conduction in both the water and the gas, and the tube is rigid.* The computing diagram is sketched in Fig. 8. As the length occupied by the gas is much smaller than that by the water,

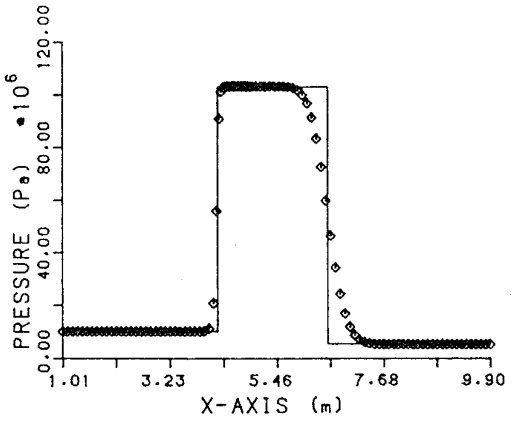

FIG. 5. The Godunov scheme for (7.2c), $t = 0.00101$.

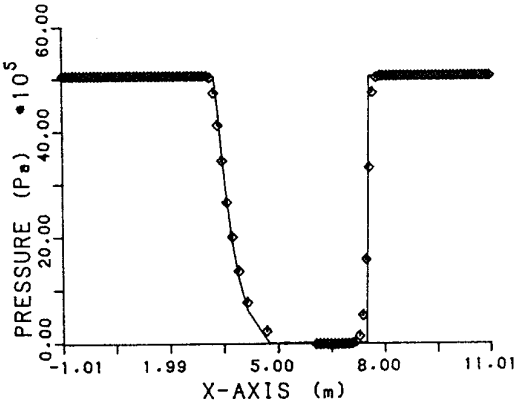

FIG. 3. Solutions for (7.2c) at $t = 0.00101$. There is a vacuum between gas and water.

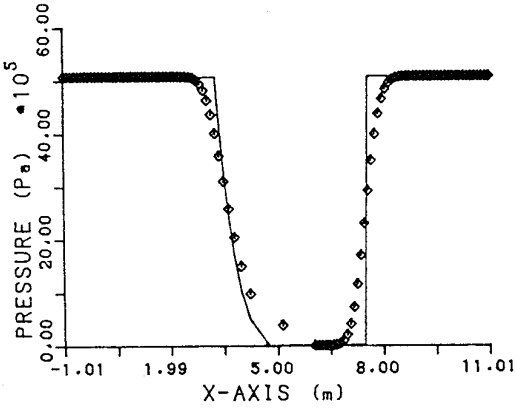

FIG. 6. The Godunove scheme for 7.2d), $t = 0.00101$.

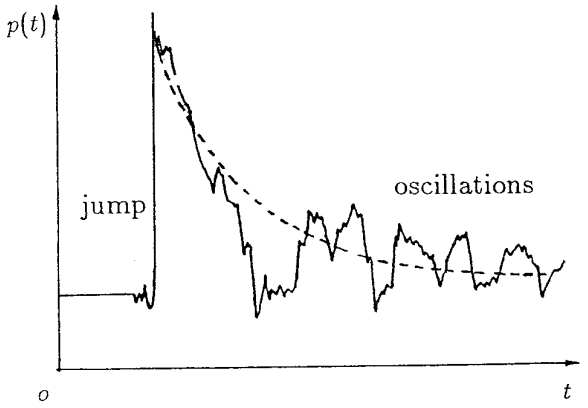

FIG. 7. Pressure at the end of the water shock tube [8].

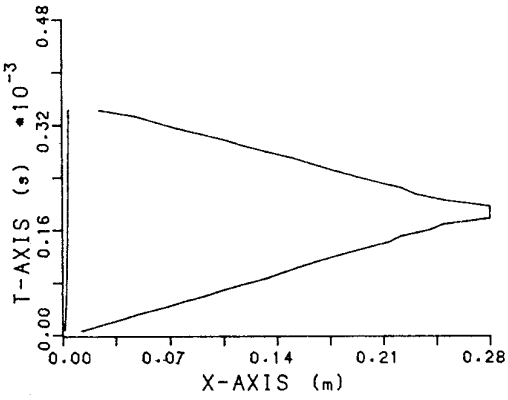

FIG. 9. Paths of the gas-water interface (the left line) and the shock in water (the right line).

an equal grid spacing is adopted in the gas and, from the interface, grid spacing is enlarged in geometrical progression in the water. The total cell number used is 100, four cells for the gas and 96 cells for the water. According to the above assumptions and the data proposed in [8], initial conditions are set as

$$U_{t=0} = \begin{cases} 70.735, 0, 100692985.3), & 0 \le x < L_1, \\ (1000, 0, 101325), & L_1 \le x \le L_2. \end{cases} \tag{7.3}$$

L_1 should be as short as possible. We chose $L_1 = 0.001$, $L_2 = 0.275$, and $\gamma = 2$. The boundary conditions are

$$\begin{aligned} x &= 0, \quad u = 0, \\ x &= L_2, \quad u = 0. \end{aligned} \tag{7.4}$$

Numerical results show that, at the beginning, the gas expands and a shock wave propagates into the water and then gradually decays in strength as depicted in Figs. 9 and 10. After the shock, which has reflected at the tube end, reaches the gas–water interface, a low pressure wave in a V shape (a pressure trough) is formed in the water and propagates to the right (Fig. 11). In this wave, water is

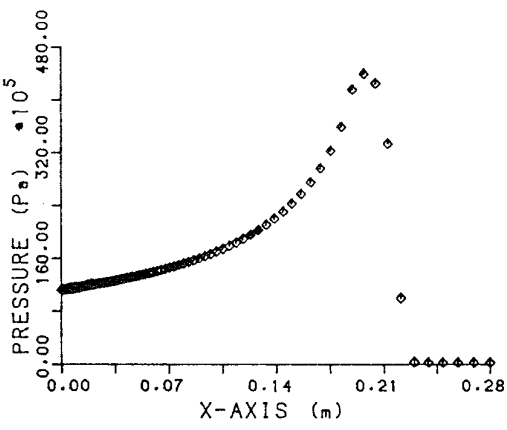

FIG. 10. The shock propagates in water and its strength reduces gradually, $t = 0.00013$.

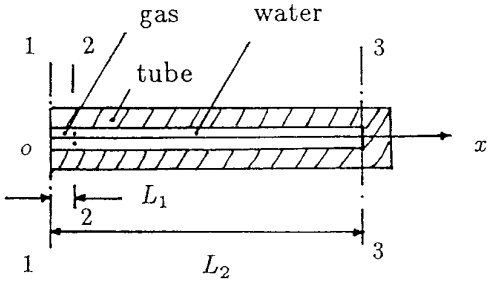

FIG. 8. The computing diagram. Owing to symmetry, only the flow in the right half of the water shock tube is calculated.

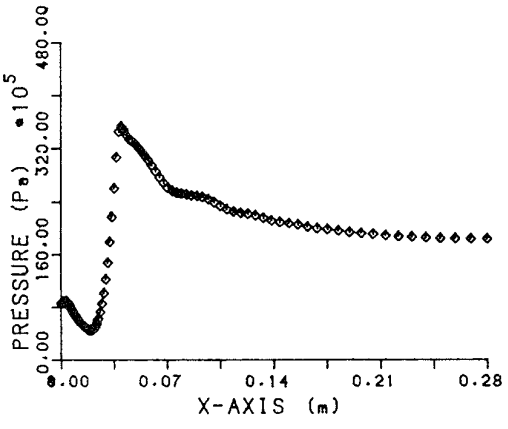

FIG. 11. A low pressure wave is formed near the gas–water interface.

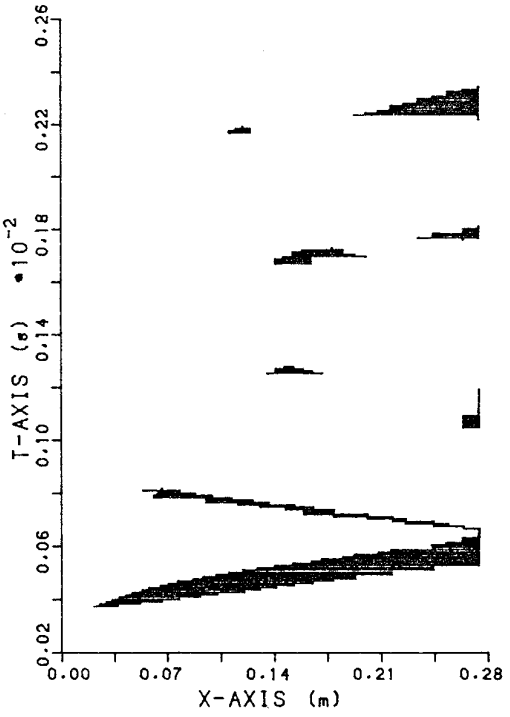

FIG. 12. Cavitation zones, $p_v = 0$. In the shadows water cavitates.

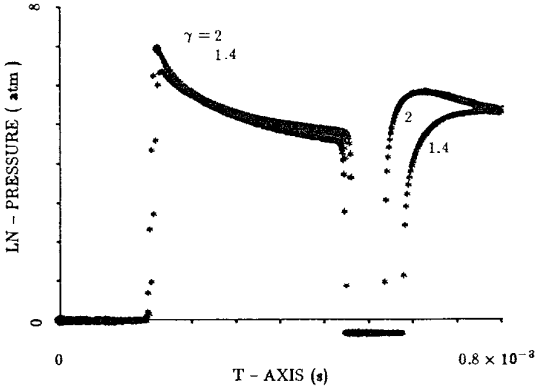

FIG. 14. Pressure at the end obtained with a TVNI scheme, moving grids, and $p_v = 1.013 \times 10^5$ [10].

rarefied and pressure develops lower and lower. At last, the water at the bottom of the wave ruptures and cavitation takes place. In Fig. 12, the cavitation zones in x–t plane is presented, and it is shown that the low pressure wave, which contains the cavitation zones, goes back and forth in the water. As illustrated in Figs. 12 and 13, the time process of pressure at the end consists of many almost isolated impulses whose occurrences correspond to the movement of the wave. The first impulse begins when the shock arrives at the end and terminates abruptly when the wave touches it. As the low pressure wave propagates away from there, the second impulse starts. Results in Fig. 13 agree with those of our early work given in Fig. 14 [10]. If the water is capable of supporting tensile stresses, i.e., $p_v < 0$, both occurrence and disappearance of a cavitation zone can generate shocks. As a result, although there are less cavitation zones, the end pressure behaves in a more oscillatory manner (Fig. 15, Fig. 16). Hence, we conclude that it is the low pressure wave that leads an end pressure to decay with multiple jumps and drops, and the cavitation process has a significant effect on the resulting flow. It should be noted that since our computations are based on a simple one-dimensional model ignoring many secondary effects, they cannot explain all the features of the flow. In the computations, CFL = 1, the algorithm (6.9) and (6.10), which act only when and where the water cavitates, are adopted for $p_v = 0$ and $p_v < 0$, respectively.

We test the effectiveness of the algorithms for the lower bound of density proposed in Section 6 by calculations with 6000 time steps and $p_v = -5.066 \times 10^6$. The lowest computed pressure of all water slabs and all the time steps without such an algorithm is -5.219×10^6, lower than p_v.

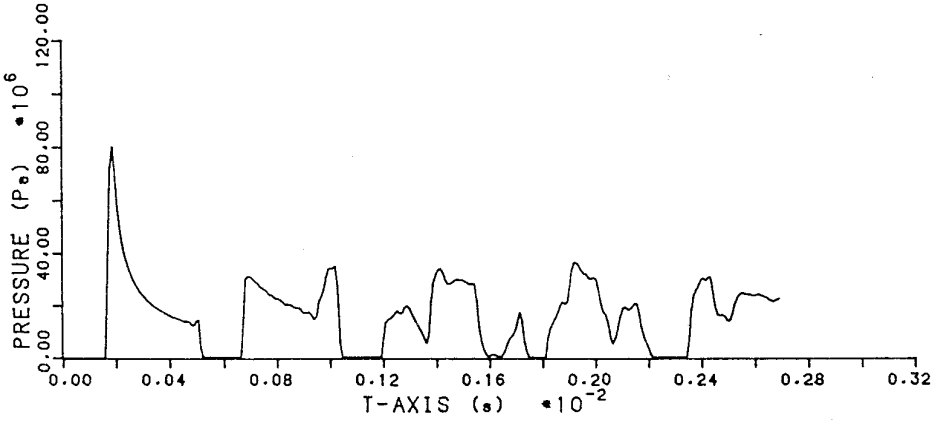

FIG. 13. Pressure at the end, $p_v = 0$.

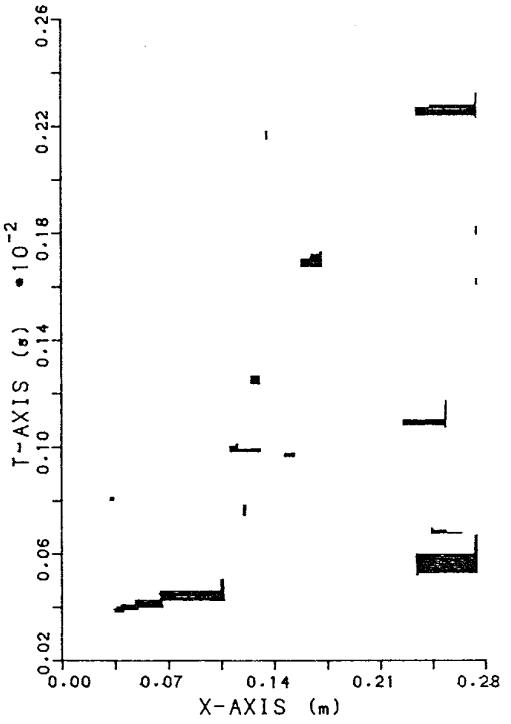

FIG. 15. Cavitation zones, $p_v = -5.066 \times 10^6$.

But by (6.9), (6.10), and (6.11b), these are, respectively, -5.049×10^6, -5.066×10^6, and -5.096×10^6, which are closer to p_v.

8. CONCLUDING REMARKS

The numerical method we propose in this paper, i.e., the E-MUSCL scheme, plus the algorithms for the lower bound of density, is a capturing method for nonlinear gas–water–vacuum systems, and it can simulate a flow process from the rarefied to vacuum state. The method has, in general, second-order accuracy and provides essentially monotone solutions. The computed results of gas–water Riemann problems demonstrate that it gives high resolution for shock waves and contact discontinuities, and good accuracy for cavitation zones as well. The numerical simulation in Section 7 also helps us to understand the flow phenomenon inside the water shock tube. It is expected that the E-MUSCL scheme, with the aid of an operator splitting technique, may be applied to some cylindrical or spherical cases, and we shall make these the subjects of further research.

ACKNOWLEDGMENTS

This paper was sponsored by the National Natural Science Foundation of China, the National Committee of Science and Technology of China, and the Doctoral Program Foundation of Institution of High Education of China. We are grateful to Professors M. W. Zhu, D. Y. Li, J. H. Wang, J. P. Chi, L. A. Ying, and Dr. B. X. Jing for helpful discussions.

REFERENCES

1. L. I. Sedov, *Similarity and Dimensional Methods in Mechanics* (Academic Press, New York, 1959) (Engl. transl.).
2. A. H. Cole, *Underwater Explosion* (Dover, New York, 1965).
3. M. Holt, Underwater explosion, *Annu. Rev. Fluid Mech.* **9,** 187 (1977).
4. A. I. Rookov, *Numerical Method of Characteristics for One-Dimensional Gas Dynamics*, Shanghai Sci. Technel., Shanghai, 1960 (Chinese transl.).
5. D. Huang and Q. S. Han, Research Report, Math and Mech. Dept., Peking University, 1964 (unpublished).
6. J. Flores and M. Holt, *J. Comput. Phys.* **44,** 377 (1981).
7. Y. L. Zhou, *Chinese Adv. in Math.* **48,** 131 (1981).
8. M. W. Zhu and X. J. Wen, *Proceedings 6th National Symp. on Shock Tube and Shock Wave* (Chinese Society of Theoretical and Applied Mechanics, Beijing, 1992), p. 154.
9. D. Huang and H. S. Tang, Numerical simulation of the flow caused by an explosion in a closed tube full of water, 1991 (unpublished).
10. A. Harten, *J. Comput. Phys.* **49,** 357 (1983).
11. S. K. Godunov, G. P. Prokopov, M. Y. Ivanov, and A. N. Zabrodin, *Numerical Solution of Multi-Dimensional Gas Dynamics Problems* (Science, Moscow, 1976) (Russian).

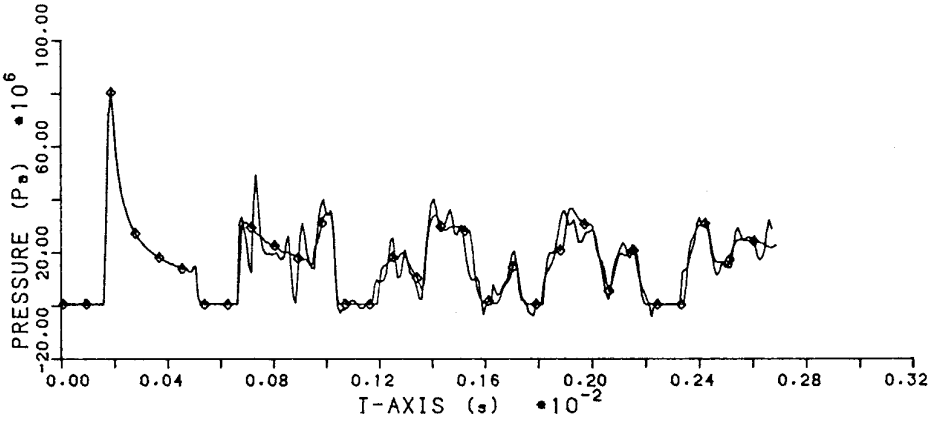

FIG. 16. Pressure at the end, $p_v = -5.066 \times 10^6$ (the line), $p_v = 0$ (the line with diamonds).

12. T. P. Liu and J. A. Smoller, *Adv. in Appl. Math.* **1,** 345 (1980).
13. J. J. Gottlieb and C. P. T. Groth, *J. Comput. Phys.* **78,** 437 (1988).
14. E. I. Babenko, *Theoretical Foundation of Numerical Algorithms for Problems of Mathematical Physics* (Main Editorial Office of Phys. & Math. Literature, Moscow, 1979) (Russian).
15. S. K. Godunov, *Math Sb.* **47,** 217 (1959) (Russian).
16. B. van Leer, *J. Comput. Phys.* **32,** 101 (1979).
17. Yu. S. Yiakovlev, *Hydrodynamics of Explosion* (State Press of Ship Industry, Leningrad, 1961) (Russian).
18. R. T. Knapp, J. W. Daily, and F. G. Hammit, *Cavitation* (McGraw–Hill, New York, 1979).
19. R. A. Wentell, H. D. Scott, and R. P. Chapman, *J. Acoust. Soc. Am.* **46,** 789 (1969).
20. P. D. Lax, *Pure Appl. Math.* **10,** 537 (1957).
21. J. A. Smoller, *Shock Waves and Reaction-Diffusion Equations* (Springer-Verlag, New York/Berlin/Heidberg, 1983).
22. Z. H. Chao, Y. D. Zhang, and R. X. Li, *Matrix Computing and Equation Solving* (China High Education Press, Beijing, 1979).